This is the accepted manuscript (postprint) of the following article:
M. Shahrouzifar, E. Salahinejad, *Strontium doping into diopside tissue engineering scaffolds*, Ceramics International, 45 (2019) 10176-10181.
https://doi.org/10.1016/j.ceramint.2019.02.067

Strontium doping into diopside tissue engineering scaffolds

M.R. Shahrouzifar, E. Salahinejad*

Faculty of Materials Science and Engineering, K. N. Toosi University of Technology, Tehran, Iran

Abstract

In this work, an inorganic-salt coprecipitation route was used to synthesize nanostructured diopside ($CaMgSi_2O_6$) powders without/with 2 mol% strontium substituted for calcium. A sponge replication technique was then employed on the powders to manufacture highly porous scaffolds with pore interconnectivity. The structure, bioactivity, biodegradation and cell adhesion of the samples were studied by X-ray diffraction, Fourier-transform infrared spectroscopy, field-emission scanning electron microscopy/energy-dispersive X-ray spectroscopy, Archimedes densitometry, and inductively coupled plasma spectroscopy analyses. According to the results, the Sr-doping process improves the sinterability and apatite-formation ability of the diopside-based scaffolds, but retards their biodegradation. Mesenchymal stem cells also present better adhesion and spreading with typical cell extensions on the Sr-doped scaffold in comparison to the pure one. It is eventually concluded that strontium can be further considered as a doping agent to improve the bioactivity and biocompatibility of Mg-Ca silicate scaffolds.

Keywords: Calcination (A); Surfaces (B); Silicate (D); Biomedical applications (E)

* Corresponding Author: Email Address: <salahinejad@kntu.ac.ir>

This is the accepted manuscript (postprint) of the following article:
M. Shahrouzifar, E. Salahinejad, *Strontium doping into diopside tissue engineering scaffolds*, Ceramics International, 45 (2019) 10176-10181.
https://doi.org/10.1016/j.ceramint.2019.02.067

1. Introduction

Mg-containing bioactive silicates are promising candidates for tissue engineering scaffolds due to their suitable mechanical properties, apatite-formation ability, biodegradation and biocompatibility [1-7]. Among this group of bioceramics, diopside ($CaMgSi_2O_6$) with excellent biocompatibility represents *in vitro* apatite-formation ability and *in vivo* bone formation ability to some extent [1-7]. That is, its bioactivity should be improved for its further medical developments.

Incorporation of proper ions into bioceramics can enhance their bioactivity, biocompatibility, mechanical and anti-bacterial properties. Typically, it has been demonstrated that doping of strontium into some bioceramics can result in higher cell proliferation and differentiation, gene expression, and bone formation [8-10]. On the one hand, some studies have proven that Sr-doped bioglasses possess higher apatite-formation ability than the undoped ones *in vitro* [11-13]. In this regard, it has been reported that the thickness of the apatite layer formed on the Sr-doped bioglass surface is thinner; nevertheless, the kinetics of the evolution of the Ca/P ratio for this type of calcium phosphate more quickly gives rise to a bone-like apatite phase. O'Donnell and Hill [14] pointed out that the larger radius of Sr in comparison to Ca is responsible for the higher reactivity of bioactive glasses *in vitro* and *in vivo* as a result of Sr doping. In fact, the entrance of Sr expands the glass network and leads to further ion release [15]. On the other hand, Sriranganathan et al. [16] found that the substitution of Ca by Sr beyond a certain amount in high-phosphate bioactive glasses impedes the formation of octacalcium phosphate and reduces the bioactivity of the glasses. Similarly, Wu et al. [17] evidenced that Sr substitution for Ca in $CaSiO_3$ reduces the ceramic dissolution. Because more lattice space is occupied and thereby ion release is reduced, due to the larger radius of Sr^{2+} with respect to Ca^{2+}. Moreover, Hesaraki et al. [18] studied the effect

This is the accepted manuscript (postprint) of the following article:
M. Shahrouzifar, E. Salahinejad, *Strontium doping into diopside tissue engineering scaffolds*, Ceramics International, 45 (2019) 10176-10181.
https://doi.org/10.1016/j.ceramint.2019.02.067

of SrO substitution for CaO up 10 mol% on the biological properties of SiO_2–CaO–P_2O_5 bioglass. Despite the increase in the dissolution rate by rising the SrO content, the apatite-formation ability was decreased. This was attributed to the fact that strontium blocks nucleation sites of amorphous calcium phosphate and delays the apatite formation.

In conclusion, the incorporation of Sr leads to different influences on the bioactivity, depending on the chemical composition and structure of the host bioceramic. To the best of our knowledge, no study has been reported on Sr-doping into diopside. Thus, in this study, Sr was replaced with Ca in diopside at 2% mol by a wet chemical route, and then macroporous Sr-doped/undoped diopside scaffolds were prepared via a sacrificial sponge replication method. Then, the resultant structure, biodegradation, apatite-formation ability and cell adhesion of the scaffolds were evaluated *in vitro*.

2. Experimental procedure

2.1. Synthesis of powders

Diopside powders were synthesized by a coprecipitation route using chloride precursors, based on Refs. [19-21]. Calcium chloride ($CaCl_2$, Merck, > 98%), magnesium chloride ($MgCl_2$, Merck, > 98%) and silicon tetrachloride ($SiCl_4$, Merck, > 99%) as the raw precursors and strontium chloride ($SrCl_2$, Merck, > 98%) as the doping agent were used. Also, dry ethanol (C_2H_5OH, Merck, > 99%) and aqueous ammonia solution (NH_4OH, Merck, 25%) were utilized as the solvent and precipitating agent, respectively. Briefly, $CaCl_2$ and $MgCl_2$ were dissolved at a same molar in a proper amount of ethanol in an ice-water bath. After the solution became clear, $SiCl_4$ was added to the solution at two times the molar amount of the magnesium and calcium chloride salts, according to the diopside stoichiometric ratio. A proper amount of ammonia solution was then added to the solution

This is the accepted manuscript (postprint) of the following article:
M. Shahrouzifar, E. Salahinejad, *Strontium doping into diopside tissue engineering scaffolds*, Ceramics International, 45 (2019) 10176-10181.
https://doi.org/10.1016/j.ceramint.2019.02.067

until pH reached 10. After drying the obtained white precipitates at 100 °C for 6 h in an oven, they were calcined at 700 °C for 2 h. The synthesis of Sr-doped diopside was similar to undoped one with a difference that 2 mol% $CaCl_2$ was replaced by the same molar amount of $SrCl_2$ to obtain the composition of $Ca_{0.98}Sr_{0.02}MgSi_2O_6$.

2.2. Fabrication of scaffolds

To manufacture scaffolds with interconnected pores, a sponge replication method was used. For the preparation of ceramic slurries, the undoped and doped diopside powders were separately suspended in 6 wt% polyvinyl alcohol (PVA) aqueous solution by a magnetic stirrer, followed by sonication. Polyurethane foams with the open porosity of approximately 25 pore per inch (ppi) were chosen as the template. After cutting the polyurethane foams into desired shapes, the foams were immersed in the slurries and then compressed, so that the slurries penetrated into the polymeric foams. The excess slurries were blown out with a compressed air flow to avoid closing the pores. Afterwards, pre-impregnated foams were dried by blowing of a mild warm wind flow at 60 °C. After drying, the coated foams were heat-treated at 400 °C for 90 min to remove the polyurethane foam template without collapsing the dried body and then sintered at 1200 °C for 3 h at a heating rate of 5 °C/min. The same heat treatment process was also applied on some of the powders synthesized by the coprecipitation method.

2.3. Structural characterization of powders and scaffolds

The powders calcined with the heat treatment regime of the scaffolds were analyzed by X-ray diffraction (XRD, CuKα) for phase characterization. Fourier-transform infrared spectroscopy (FTIR) was also used for bonding identification, especially the confirmation of

This is the accepted manuscript (postprint) of the following article:
M. Shahrouzifar, E. Salahinejad, *Strontium doping into diopside tissue engineering scaffolds*, Ceramics International, 45 (2019) 10176-10181.
https://doi.org/10.1016/j.ceramint.2019.02.067

the incorporation of Sr into the diopside structure. The morphology of the sintered scaffolds was also investigated by field-emission scanning electron microscopy (FESEM). To measure the porosity percent of the scaffolds (*P*), the water Archimedes method was used based on the following formula:

$$P\ (\%)\ = (W_2 - W_1)/(W_2 - W_3) \times 100 \quad (1)$$

where W_1 is the weight of the scaffolds in air, W_2 is the weight of the scaffolds with water, and W_3 is the weight of the scaffolds suspended in water, conducted in three replicates.

2.4. Apatite-formation ability and degradation evaluations of scaffolds

For the assessment of the effect of Sr-doping on *in vitro* apatite-formation ability, the sintered scaffolds were soaked in the simulated body fluid (SBF) for 7 days at 37 °C. The ratio of the solution volume to the scaffold mass was chosen equal to 200 ml.g^{-1}. After immersion, the scaffolds were dried at room temperature for 3 days and then studied by FESEM equipped with energy-dispersive X-ray spectroscopy (EDS).

After 7 days of immersion, the concentration of principal ions in the SBF was also measured by inductively coupled plasma spectroscopy (ICP). As the initial SBF has no Si ions, the concentration of Si ions in the SBF after immersion was employed as a criterion for measuring the weight loss of the scaffolds (*d*), using the following equation:

$$d = (C_{Si} \times V_S)/\ m_{Si} \times 100 \quad (2)$$

where C_{Si}, V_S and m_{Si} represent the concentration of Si in the SBF, the volume of the SBF (ml) and the Si content (mg) of the samples immersed in the SBF, respectively.

2.5. Cell adhesion studies on scaffolds

This is the accepted manuscript (postprint) of the following article:
M. Shahrouzifar, E. Salahinejad, *Strontium doping into diopside tissue engineering scaffolds*, Ceramics International, 45 (2019) 10176-10181.
https://doi.org/10.1016/j.ceramint.2019.02.067

For evaluating cell attachment on the surface of the fabricated scaffolds, they were sterilized by immersing in an ethanol solution (70%) for 3 h, followed by washing with phosphate-buffered saline (PBS). The sterilization process was terminated by exposing the scaffolds to a UV radiation for 20 min. Mesenchymal stem cells (MSCs) were seeded onto the sterilized scaffolds in a 24-well plate in a humidified medium with the atmosphere of 95% air and 5% CO_2 at 37 °C. After 24 h of culture, the scaffolds were removed from the culture wells and rinsed twice with PBS. The cells on the scaffolds were then fixed with 2.5% glutaraldehyde. After 1 h, the scaffolds were rinsed with PBS to remove glutaraldehyde. Then, the scaffolds were dehydrated twice in a grade ethanol series for 10 min. The dehydration process was completed by placing the scaffolds under a laminar flow hood for 24 h. Finally, the cells on the surfaces were observed by SEM.

3. Results and discussion

3.1. Structural characterization

The XRD patterns of the powders calcined with the scaffolding heat procedure are shown in Fig. 1. As can be seen, both patterns merely indicate the characteristic peaks of single-phase diopside. Hence, it is concluded from the XRD analysis that, on the one hand, the coprecipitation and calcination processes used in this work successfully develop a single-phase diopside structure. On the other hand, the incorporation of Sr^{2+} into diopside at this level does not result in the formation of any additional phases.

Fig. 2 depicts the FTIR spectra of the calcined powders to check the phase analysis conducted by XRD and the incorporation of Sr into the structure. In the undoped sample, the peaks of 476 and 518 cm^{-1} are assigned to the non-bridging bending vibrations of O-Mg-O. The two sharp peaks of 636 and 674 cm^{-1} and two other peaks at 867 and 924 cm^{-1}

This is the accepted manuscript (postprint) of the following article:
M. Shahrouzifar, E. Salahinejad, *Strontium doping into diopside tissue engineering scaffolds*, Ceramics International, 45 (2019) 10176-10181.
https://doi.org/10.1016/j.ceramint.2019.02.067

correspond to the non-bridging bending vibration of O-Si-O and non-bridging stretching mode of Si-O, respectively. The peaks of around 969 and 1083 cm^{-1} are also attributed to the stretching vibrations of Si-O. All the detected FTIR peaks are in good agreement with the vibrations of the functional groups of diopside [22, 23], confirming the XRD analysis. For Sr-doped diopside, the non-bridging bending vibrations of O-Mg-O are located at 478 and 518 cm^{-1}, i.e. a slight shift for one of the peaks in comparison to pure diopside. Except the peak shift of the bridging stretching vibration of Si-O to 1078 cm^{-1}, the other major part of the Si-O vibrations exhibit no wavenumber shifts. Based on the central force model [24], the change in the position of the stretching vibration frequency of Si-O can be attributed to structural variations related to changes in the angle of the O-Si-O bond in the tetrahedral spaces. Since Sr^{2+} has a larger ionic radius than Ca^{2+}, this partial replacement can cause changes in the angle of O-Si-O bond and thereby changes in the vibrational frequency bond. In fact, due to doping into the silica network, a structural rearrangement happens and inter-tetrahedral angle values are reduced. Owing to this decrease in the local symmetry of the Si-O bond, its vibrational frequencies change [25], which can be regarded as a typical evidence for the incorporation of Sr into the diopside structure.

The pore morphology and level of the scaffolds were assessed by Archimedes densitometric and microscopic methods. According to the water Archimedes method, the porosity level of the undoped and doped diopside scaffolds is 90.7± 2.6 and 92.7±1.2 %, respectively. Also, as depicted in Figs. 3(a) and 3(b), both scaffolds possess open and interconnected pores. The smallest diameters of pores in the undoped and doped scaffolds are about 377 and 416 µm and the biggest diameter are 763 and 805 µm, respectively. The median diameters of pores in the undoped and doped scaffolds are 550 and 502 µm, respectively. It would be worth mentioning that the dimensions of pores in the fabricated

This is the accepted manuscript (postprint) of the following article:
M. Shahrouzifar, E. Salahinejad, *Strontium doping into diopside tissue engineering scaffolds*, Ceramics International, 45 (2019) 10176-10181.
https://doi.org/10.1016/j.ceramint.2019.02.067

samples satisfy the requirement of issue engineering scaffolds. Such hierarchical porous structures with a large surface-to-volume ratio and pores of at least 100 µm in diameter provide desired cell penetration, tissue in-growth, vascularization and nutrient transport [26, 27]. Figs. 3(c) and 3(d) also indicates the high-magnification FESEM micrograph taken of struts of the sintered scaffolds. As it is clear, the struts are composed on irregular-shaped diopside particles of 50-500 nm in size, with a nanometric porous feature. This micro/nanoporous nature of the scaffolds, as well as the nanometer-to-micron sizes of the particles, beneficially provide a high specific area which is essential for bioactivity. Also, it can be seen that particle boundaries in the Sr-doped sample are less distinguishable than the undoped one, which is indicative of the improved level of particle coalescence and necking. It suggests that Sr-doping into diopside improves sinterability. On the one hand, Sr^{2+} possesses a larger ionic radius (1.13 Å) than Ca^{2+} (1 Å) [28], which causes an increase in the lattice parameters of diopside due to the partial substitution of these two ions. This facilitates ionic mobility at high temperatures [17]. On the other hand, the improved sinterability as a result of Sr-doping can be attributed to the increase of the homologous temperature or the decrease of the effective sintering temperature. The field strength of Sr^{2+} ion (1.44) is lower than Ca^{2+} (2.04) [29, 30]; thus, Sr^{2+} substation for Ca^{2+} can weaken the crystal structure of diopside and lower the sintering temperature. It means that at a given temperature, the Sr-doped scaffolds experience a higher homologous temperature than pure diopside. In agreement with this argument, Massera and Hupa [31] showed that by increasing the substitution of SrO for CaO in S53P4 bioactive glass, the sintering temperature decreases in consequence of the field strength reduction.

3.2. Apatite formation ability and degradation

This is the accepted manuscript (postprint) of the following article:
M. Shahrouzifar, E. Salahinejad, *Strontium doping into diopside tissue engineering scaffolds*, Ceramics International, 45 (2019) 10176-10181.
https://doi.org/10.1016/j.ceramint.2019.02.067

Fig. 4 shows the FESEM micrographs and EDS patterns of the scaffolds after 7 days of soaking in the SBF. Based on the low-magnification micrographs (Figs. 4(a) and 4(b)), a good number of apatite spheres are formed on the surfaces of the Sr-doped scaffolds, whereas merely sparse plates of apatite are observed on the surface of the pure diopside scaffold. The mean diameter of the apatite spheres on the doped scaffold and the average thickness of the apatite plates on the pure one are 1.58 μm and 32.6 nm, respectively. It means that the Sr-doped scaffold presents a better apatite-formation ability in comparison to the undoped one. Also, according to Figs. 4(c) and 4(d), both the formed apatites possess a leaf-like morphology. Concerning the EDS analysis presented in Figs. 4(e) and 4(f), the peak intensity of phosphorous for both the two immersed scaffolds is almost the same, but the quantitative amount of phosphorous detected on the soaked doped scaffold (12.8 wt%) is more than that of the undoped one (10.15 wt%). This is another evidence for the higher apatite-formation ability of doped diopside. The EDS analysis of the surfaces also represents the existence of Si and Mg belonging to diopside. It dictates that the detected Ca originates from both diopside and apatite; thus, the Ca/P ratio cannot be used to characterize the type of apatite precipitates.

The *in vitro* biodegradation of the scaffolds was also evaluated by the ICP analysis of the SBFs before and after immersion of the samples. Table 1 lists the ionic concentration of Ca, Si, Mg, Sr and P before and after 7 days of contact with the scaffolds. In comparison to the fresh SBF, the concentration of Ca for both scaffolds was increased, which is an evidence for the degradation of Ca from the scaffolds toward the EBF. In addition, this ion is critically involved in the precipitation of apatite (calcium phosphate) on the scaffold surfaces. Thus, the only conclusion which can be drawn from the increase of the Ca concentration is that the Ca degradation prevails over the Ca precipitation occurring during the apatite deposition. The increase observed in the concentration of Si and Mg is merely controlled by the scaffold

This is the accepted manuscript (postprint) of the following article:
M. Shahrouzifar, E. Salahinejad, *Strontium doping into diopside tissue engineering scaffolds*, Ceramics International, 45 (2019) 10176-10181.
https://doi.org/10.1016/j.ceramint.2019.02.067

dissolution into the SBF, since these two ions do not cooperate in the apatite formation. It can be seen that the increases for the Sr-doped diopside sample are lower than those for the pure one. Since the fresh SBF does not contain Si, the concentration of Si ion in the SBF after immersion can be utilized as a criterion for measuring the weight loss of the scaffolds. Table 2 tabulates the weight loss of the scaffolds after incubation in the SBF until the 7^{th} day, indicating the lower degradation of the Sr-doped diopside scaffold. The lower release of Si and Mg ions into the SBF for Sr-doped diopside can be attributed to the larger radius of Sr^{2+} than Ca^{2+}, which occupies more vacant spaces in the crystal lattice and retards the movement and release of these ions. Additionally, the improved sinterability due to Sr-doping, as addressed above, can have a contribution to the decrease of the ion release, via the decrease in the surface area of the scaffolds exposed to the SBF. More importantly, since diopside possesses no phosphorous, the reduction in the P content of the SBF due to contact with the scaffolds demonstrates the level of the apatite-formation ability of the immersed scaffolds. In this regard, the more consumption of P of the SBF after immersion shows further apatite-formation ability on the surface of the scaffolds. That is, the ICP analysis verified the higher apatite-formation ability of the Sr-doped sample in comparison to the undoped scaffold, as realized in the FESEM and EDS studies.

In general, the bioactivity of bioceramics depends on their chemical composition, crystallinity, density and porosity structure [32, 33]. Based on Fig. 3, the addition of Sr into diopside improves the sinterability and coalescence of particles. This improvement in the sintering process causes the reduction of texture pores, which alone results in a negative effect on apatite-formation ability via reducing reactivity. However, the observed improvement in *in vitro* bioactivity due to Sr-doping suggests that the role of chemical

This is the accepted manuscript (postprint) of the following article:
M. Shahrouzifar, E. Salahinejad, *Strontium doping into diopside tissue engineering scaffolds*, Ceramics International, 45 (2019) 10176-10181.
https://doi.org/10.1016/j.ceramint.2019.02.067

composition prevails over that of the porosity level, which can be considered from several viewpoints:

1) The incorporation of Sr into diopside enhances the apatite-formation ability of diopside, via reducing the release level of Mg^{2+}, as explored by the ICP results. Based on the literature [34-36], the presence of MgO greater than 7% mol in silicate-phosphate glasses retards their apatite-formation ability. Indeed, Mg^{2+} ions released in the SBF inhibits the formation of calcium phosphate layer and then its conversion into hydroxyapatite. This fact arises from competitive bonds between magnesium and phosphate ions on the glass surface [37].
2) The increase of non-bridging oxygen groups in the silicate structure owing to the addition of Sr, as realized from the FTIR analysis, has a positive effect on the *in vitro* bioactivity of diopside. As can be seen in the FTIR spectrum of Sr-doped diopside (Fig. 2(b)), the peak intensity of the non-bridging functional groups of Si-O at 867 and 923 cm^{-1} is decreased in comparison to pure diopside. It should be, however, noted that the FTIR data in Fig. 2 is expressed in terms of transmittance. That is, the decrease in the transmittance intensity of non-bridging functional groups is equivalent to the increase of the absorbance percentage, suggesting the weakening of the silica network with a decrease in the local symmetry of the non-bridging Si-O functional groups in terms of the Sr cohesivity to the lattice. Because of the larger size of Sr^{2+} in comparison to Ca^{2+}, the smaller ratio of electric charge to size (lower ionic field strength) for Sr^{2+} causes a weaker bond with silicate (SiO_4^{4-}). Therefore, Sr^{2+} which connects to silicates in the two chains of $Si_2O_6^{4-}$ as a network modifier can be more effectively exchanged with H^+ or H_3O^+ as the first step of the bioactivity reaction. This leads to the development of more silanol (Si-OH) groups on the surface, which plays a significant role in the nucleation of

This is the accepted manuscript (postprint) of the following article:
M. Shahrouzifar, E. Salahinejad, *Strontium doping into diopside tissue engineering scaffolds*, Ceramics International, 45 (2019) 10176-10181.
https://doi.org/10.1016/j.ceramint.2019.02.067

apatite [38]. Similarly, Vers et al. [39] investigated the influence of the substitution of ZnO for CaO in $60SiO_2.(35\text{-}x)\ CaO.xZnO.5P_2O_5$ glass-ceramics with x = 3, 7, 10 mol% on bioactivity. According this study, the FTIR peak intensity of Si-ONB (three non-bridging oxygen per SiO_4 tetrahedron-Q^1 groups) and Si-O2NB (two non-bridging oxygen per SiO_4 tetrahedron-Q^2 groups) vibrations is increased with the increase of the ZnO concentration, accompanied by a net decrease in the local symmetry of the vitreous silica network. This increase in transmittance means the decrease of absorbance and thereby bioactivity as a result of substitution of ZnO for CaO.

3.3. Cell adhesion

Fig. 5 shows the morphology of MSCs cultured on the undoped and Sr-doped scaffolds after 24 h of incubation. On both scaffolds, the cells were flat and spread with extensions; however, the cell attachment and spreading on the Sr-doped scaffold are more extended and homogeneous compared to the pure one. On the surface of the Sr-doped scaffold, some cytoplasmic bridges of MSCs are also seen. It means that the addition of strontium into diopside improves the cell adhesion, which can be discussed from several aspects.

As found in the ICP studies, the amount of ion release from the Sr-doped scaffold is lower than the pure one. The fast release of ions coupled with surface reactions can have a negative effect on the protein adsorption and hence cell adhesion at the early stage of incubation. This can be regarded as an indirect positive contribution of Sr to cell adhesion. But from a direct viewpoint, Bonnelye et al. [40] reported that Sr^{2+} stimulates the osteoblastic activity of mouse calvaria cells *in vitro*, when the concentration of Sr^{2+} in the medium is below 87.6 ppm. In the current study, the concentration of Sr^{2+} is 18.97 ppm until 7th day of culture, which means that the cell adhesion benefits from this level of Sr in the environment.

This is the accepted manuscript (postprint) of the following article:
M. Shahrouzifar, E. Salahinejad, *Strontium doping into diopside tissue engineering scaffolds*, Ceramics International, 45 (2019) 10176-10181.
https://doi.org/10.1016/j.ceramint.2019.02.067

The improvement in the apatite-formation ability of diopside as a result of Sr-doping, as realized from the SEM/EDS and ICP analysis, also can encourage protein adsorption and then cell adhesion, because of the desirable biocompatibility characteristics of apatite [41].

4. Conclusions

In this study, highly porous pure and Sr-doped diopside scaffolds with a large pore size and high interconnectivity were successfully prepared via coprecipitation and polymer foam replication methods. The following conclusions were drawn from this work:

1) Incorporation of Sr^{2+} for 2 mol% did not cause the formation of any second phases.

2) The powder particle sinterability was improved due to Sr-doping.

3) The apatite-formation ability of the scaffolds was increased by the addition of 2% mol Sr^{2+} into diopside, whereas the biodegradation was decreased.

4) Sr-doping into diopside led to an improvement in the adhesion and spreading of MSCs.

References

[1] T. Nonami, S. Tsutsumi, Study of diopside ceramics for biomaterials, Journal of Materials Science: Materials in Medicine, 10 (1999) 475-479.
[2] T. Kobayashi, K. Okada, T. Kuroda, K. Sato, Osteogenic cell cytotoxicity and biomechanical strength of the new ceramic Diopside, Journal of Biomedical Materials Research: An Official Journal of The Society for Biomaterials and The Japanese Society for Biomaterials, 37 (1997) 100-107.
[3] Y. Miake, T. Yanagisawa, Y. Yajima, H. Noma, N. Yasui, T. Nonami, High-resolution and analytical electron microscopic studies of new crystals induced by a bioactive ceramic (diopside), Journal of dental research, 74 (1995) 1756-1763.
[4] N.Y. Iwata, G.-H. Lee, Y. Tokuoka, N. Kawashima, Sintering behavior and apatite formation of diopside prepared by coprecipitation process, colloids and surfaces B: Biointerfaces, 34 (2004) 239-245.
[5] W. Zhai, H. Lu, C. Wu, L. Chen, X. Lin, K. Naoki, G. Chen, J. Chang, Stimulatory effects of the ionic products from Ca–Mg–Si bioceramics on both osteogenesis and angiogenesis in vitro, Acta biomaterialia, 9 (2013) 8004-8014.
[6] N. Esmati, T. Khodaei, E. Salahinejad, E. Sharifi, Fluoride doping into SiO2-MgO-CaO bioactive glass nanoparticles: bioactivity, biodegradation and biocompatibility assessments, Ceramics International, 44 (2018) 17506-17513.

[7] H. Rahmani, E. Salahinejad, Incorporation of monovalent cations into diopside to improve biomineralization and cytocompatibility, Ceramics International, 44 (2018) 19200-19206.
[8] H. Zreiqat, Y. Ramaswamy, C. Wu, A. Paschalidis, Z. Lu, B. James, O. Birke, M. McDonald, D. Little, C.R. Dunstan, The incorporation of strontium and zinc into a calcium–silicon ceramic for bone tissue engineering, Biomaterials, 31 (2010) 3175-3184.
[9] T.C. Schumacher, A. Aminian, E. Volkmann, H. Lührs, D. Zimnik, D. Pede, W. Wosniok, L. Treccani, K. Rezwan, Synthesis and mechanical evaluation of Sr-doped calcium-zirconium-silicate (baghdadite) and its impact on osteoblast cell proliferation and ALP activity, Biomedical Materials, 10 (2015) 055013.
[10] P.K. Khan, A. Mahato, B. Kundu, S.K. Nandi, P. Mukherjee, S. Datta, S. Sarkar, J. Mukherjee, S. Nath, V.K. Balla, Influence of single and binary doping of strontium and lithium on in vivo biological properties of bioactive glass scaffolds, Scientific reports, 6 (2016) 32964.
[11] J. Lao, J.-M. Nedelec, E. Jallot, New strontium-based bioactive glasses: physicochemical reactivity and delivering capability of biologically active dissolution products, Journal of Materials Chemistry, 19 (2009) 2940-2949.
[12] J. Lao, E. Jallot, J.-M. Nedelec, Strontium-delivering glasses with enhanced bioactivity: a new biomaterial for antiosteoporotic applications?, Chemistry of Materials, 20 (2008) 4969-4973.
[13] Y.C. Fredholm, N. Karpukhina, D.S. Brauer, J.R. Jones, R.V. Law, R.G. Hill, Influence of strontium for calcium substitution in bioactive glasses on degradation, ion release and apatite formation, Journal of The Royal Society Interface, 9 (2012) 880-889.
[14] M. O'donnell, R. Hill, Influence of strontium and the importance of glass chemistry and structure when designing bioactive glasses for bone regeneration, Acta Biomaterialia, 6 (2010) 2382-2385.
[15] Y.C. Fredholm, N. Karpukhina, R.V. Law, R.G. Hill, Strontium containing bioactive glasses: glass structure and physical properties, Journal of Non-Crystalline Solids, 356 (2010) 2546-2551.
[16] D. Sriranganathan, N. Kanwal, K.A. Hing, R.G. Hill, Strontium substituted bioactive glasses for tissue engineered scaffolds: the importance of octacalcium phosphate, Journal of Materials Science: Materials in Medicine, 27 (2016) 39.
[17] C. Wu, Y. Ramaswamy, D. Kwik, H. Zreiqat, The effect of strontium incorporation into CaSiO3 ceramics on their physical and biological properties, Biomaterials, 28 (2007) 3171-3181.
[18] S. Hesaraki, M. Gholami, S. Vazehrad, S. Shahrabi, The effect of Sr concentration on bioactivity and biocompatibility of sol–gel derived glasses based on CaO–SrO–SiO2–P2O5 quaternary system, Materials Science and Engineering: C, 30 (2010) 383-390.
[19] M.J. Baghjeghaz, E. Salahinejad, Enhanced sinterability and in vitro bioactivity of diopside through fluoride doping, Ceramics International, 43 (2017) 4680-4686.
[20] E. Salahinejad, M.J. Baghjeghaz, Structure, biomineralization and biodegradation of Ca-Mg oxyfluorosilicates synthesized by inorganic salt coprecipitation, Ceramics International, 43 (2017) 10299-10306.
[21] N. Namvar, E. Salahinejad, A. Saberi, M.J. Baghjeghaz, L. Tayebi, D. Vashaee, Toward reducing the formation temperature of diopside via wet-chemical synthesis routes using chloride precursors, Ceramics International, 43 (2017) 13781-13785.
[22] K. Omori, Analysis of infrared absorption spectrum of diopside, American Mineralogist, 56 (1971) 1607-1616.
[23] R. Choudhary, J. Vecstaudza, G. Krishnamurithy, H.R.B. Raghavendran, M.R. Murali, T. Kamarul, S. Swamiappan, J. Locs, In-vitro bioactivity, biocompatibility and dissolution studies of diopside prepared from biowaste by using sol–gel combustion method, Materials Science and Engineering: C, 68 (2016) 89-100.

[24] E. Parada, P. Gonzalez, J. Pou, J. Serra, D. Fernandez, B. Leon, M. Pérez-Amor, Aging of photochemical vapor deposited silicon oxide thin films, Journal of Vacuum Science & Technology A: Vacuum, Surfaces, and Films, 14 (1996) 436-440.
[25] J. Serra, P. Gonzalez, S. Liste, S. Chiussi, B. Leon, M. Pérez-Amor, H. Ylänen, M. Hupa, Influence of the non-bridging oxygen groups on the bioactivity of silicate glasses, Journal of Materials science: Materials in medicine, 13 (2002) 1221-1225.
[26] N. OKII, S. NISHIMURA, K. KURISU, Y. TAKESHIMA, T. UOZUMI, In vivo histological changes occurring in hydroxyapatite cranial reconstruction, Neurologia medico-chirurgica, 41 (2001) 100-104.
[27] T. Freyman, I. Yannas, L. Gibson, Cellular materials as porous scaffolds for tissue engineering, Progress in Materials Science, 46 (2001) 273-282.
[28] S.J. Saint-Jean, C. Camire, P. Nevsten, S. Hansen, M. Ginebra, Study of the reactivity and in vitro bioactivity of Sr-substituted α-TCP cements, Journal of Materials Science: Materials in Medicine, 16 (2005) 993-1001.
[29] R.C. Weast, M.J. Astle, CRC handbook of chemistry and physics, CRC, Cleveland, OH1969.
[30] L. Brewer, E. Brackett, The Dissociation Energies of Gaseous Alkali Halides, Chemical Reviews, 61 (1961) 425-432.
[31] J. Massera, L. Hupa, Influence of SrO substitution for CaO on the properties of bioactive glass S53P4, Journal of Materials Science: Materials in Medicine, 25 (2014) 657-668.
[32] I. Cacciotti, Bivalent cationic ions doped bioactive glasses: The influence of magnesium, zinc, strontium and copper on the physical and biological properties, Journal of Materials Science, 52 (2017) 8812-8831.
[33] R. Vahedifard, E. Salahinejad, Microscopic and spectroscopic evidences for multiple ion-exchange reactions controlling biomineralization of CaO. MgO. 2SiO2 nanoceramics, Ceramics International, 43 (2017) 8502-8508.
[34] J. Ma, C. Chen, D. Wang, Y. Jiao, J. Shi, Effect of magnesia on the degradability and bioactivity of sol–gel derived SiO2–CaO–MgO–P2O5 system glasses, Colloids and Surfaces B: Biointerfaces, 81 (2010) 87-95.
[35] J. Soulié, J.-M. Nedelec, E. Jallot, Influence of Mg doping on the early steps of physico-chemical reactivity of sol–gel derived bioactive glasses in biological medium, Physical Chemistry Chemical Physics, 11 (2009) 10473-10483.
[36] M. Vallet-Regi, A. Salinas, J. Roman, M. Gil, Effect of magnesium content on the in vitro bioactivity of CaO-MgO-SiO 2-P 2 O 5 sol-gel glasses, Journal of Materials Chemistry, 9 (1999) 515-518.
[37] M. Diba, F. Tapia, A.R. Boccaccini, L.A. Strobel, Magnesium-containing bioactive glasses for biomedical applications, International Journal of Applied Glass Science, 3 (2012) 221-253.
[38] C. Ohtsuki, T. Kokubo, T. Yamamuro, Mechanism of apatite formation on CaOSiO2P2O5 glasses in a simulated body fluid, Journal of Non-Crystalline Solids, 143 (1992) 84-92.
[39] R. Veres, A. Vulpoi, K. Magyari, C. Ciuce, V. Simon, Synthesis, characterisation and in vitro testing of macroporous zinc containing scaffolds obtained by sol–gel and sacrificial template methods, Journal of Non-Crystalline Solids, 373 (2013) 57-64.
[40] E. Bonnelye, A. Chabadel, F. Saltel, P. Jurdic, Dual effect of strontium ranelate: stimulation of osteoblast differentiation and inhibition of osteoclast formation and resorption in vitro, Bone, 42 (2008) 129-138.
[41] Y. Hosseini, R. Emadi, M. Kharaziha, A. Doostmohammadi, Reinforcement of electrospun poly (ε-caprolactone) scaffold using diopside nanopowder to promote biological and physical properties, Journal of Applied Polymer Science, 134 (2017) 44433.

This is the accepted manuscript (postprint) of the following article:
M. Shahrouzifar, E. Salahinejad, *Strontium doping into diopside tissue engineering scaffolds*, Ceramics International, 45 (2019) 10176-10181.
https://doi.org/10.1016/j.ceramint.2019.02.067

Tables

Table 1. ICP results of the SBFs after 7 days of contact with the scaffolds.

Type of SBF	Ion concentration (ppm)			
	Ca	Mg	Si	P
Fresh	100.2	36.6	0.0	30.9
Exposed to undoped diopside	112.9	69.2	54.1	8.3
Exposed to Sr-doped diopside	117.1	60.4	43.1	1.7

Table 2. Weight loss data of the scaffolds after 7 days of immersion in the SBF.

Scaffold Type	Scaffold mass (mg)	Volume of SBF (ml)	Si content of scaffolds (mg)	Weight loss of scaffolds (%)
Undoped diopside	0.18	35.78	46.40	4.17
Sr-doped diopside	0.11	21.82	28.17	3.33

This is the accepted manuscript (postprint) of the following article:
M. Shahrouzifar, E. Salahinejad, *Strontium doping into diopside tissue engineering scaffolds*, Ceramics International, 45 (2019) 10176-10181.
https://doi.org/10.1016/j.ceramint.2019.02.067

Figures

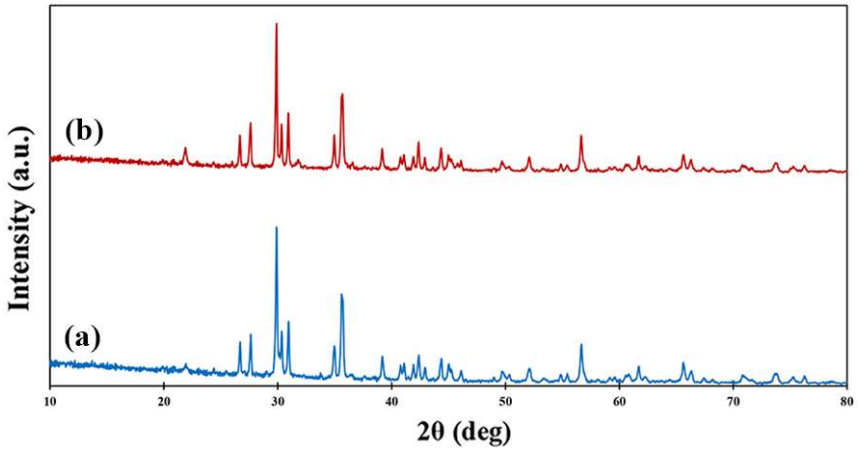

Fig. 1. XRD patterns of the undoped (a) and Sr-doped (b) diopside powders after calcination.

All the diffraction peaks belong to diopside (Ref. code: 00–017-0318).

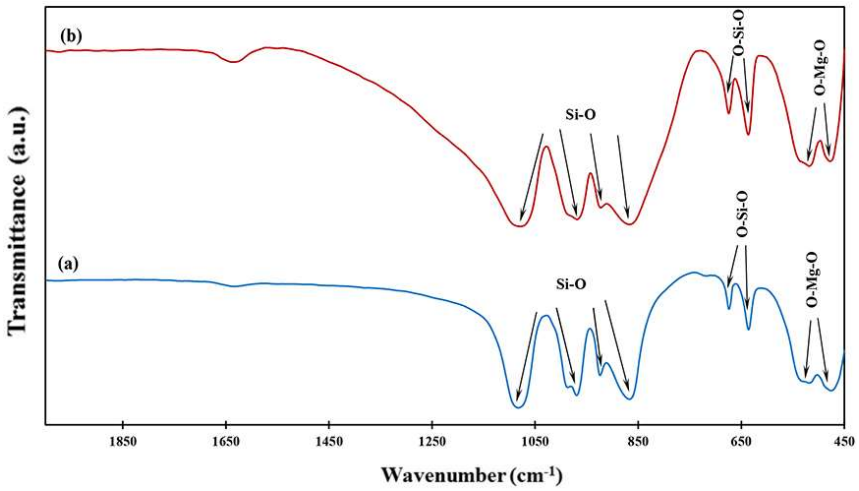

Fig. 2. FTIR spectra of the undoped (a) and Sr-doped (b) diopside powders after calcination.

This is the accepted manuscript (postprint) of the following article:
M. Shahrouzifar, E. Salahinejad, *Strontium doping into diopside tissue engineering scaffolds*, Ceramics International, 45 (2019) 10176-10181.
https://doi.org/10.1016/j.ceramint.2019.02.067

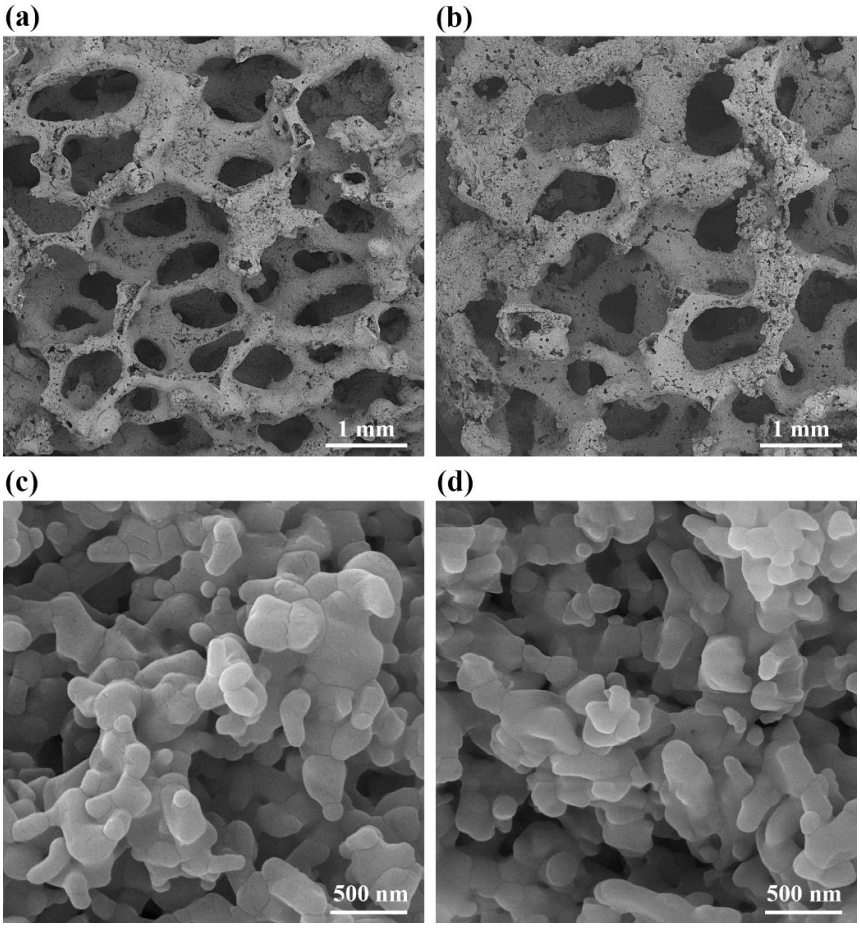

Fig. 3. Low-magnification FESEM micrographs of the undoped (a) and Sr-doped (b) diopside scaffolds and high-magnification FESEM micrographs of the undoped (c) and Sr-doped (d) diopside scaffolds.

This is the accepted manuscript (postprint) of the following article:
M. Shahrouzifar, E. Salahinejad, *Strontium doping into diopside tissue engineering scaffolds*, Ceramics International, 45 (2019) 10176-10181.
https://doi.org/10.1016/j.ceramint.2019.02.067

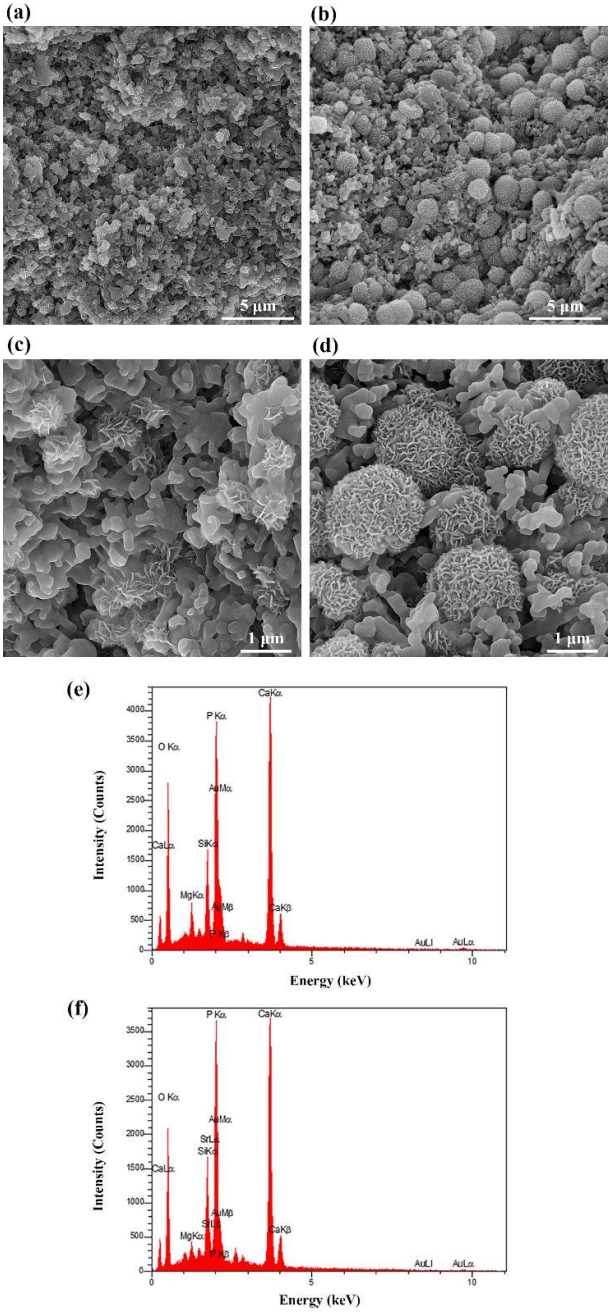

Fig. 4. Low-magnification FESEM micrographs of the undoped (a) and Sr-doped (b) diopside scaffolds, high-magnification FESEM micrographs of the undoped (c) and Sr-doped (d) diopside scaffolds, and EDS patterns taken of the undoped (e) and Sr-doped (f) diopside scaffolds after soaking in the SBF for 7 days.

This is the accepted manuscript (postprint) of the following article:
M. Shahrouzifar, E. Salahinejad, *Strontium doping into diopside tissue engineering scaffolds*, Ceramics International, 45 (2019) 10176-10181.
https://doi.org/10.1016/j.ceramint.2019.02.067

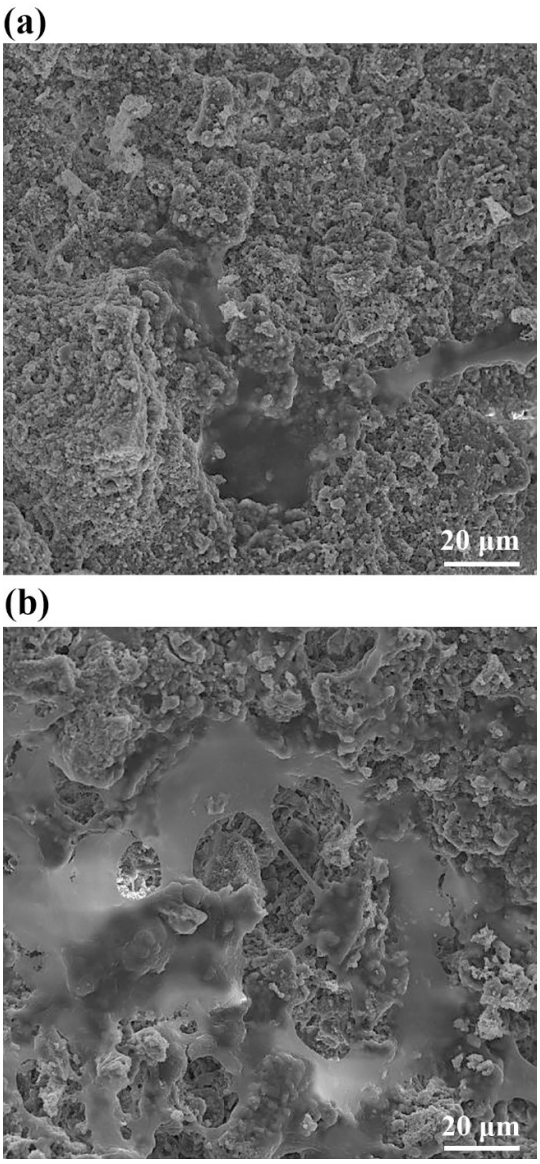

Fig. 5. SEM micrographs of cells cultured on the undoped (a) and Sr-doped (b) diopside scaffolds after 24 h of incubation.